ACSNANO

www.acsnano.org

ARTICLE

Controlled Multidirectional Particle Transportation by Magnetic Artificial Cilia

Shuaizhong Zhang, Rongjing Zhang, Ye Wang, Patrick R. Onck,* and Jaap M. J. den Toonder*

Cite This: https://dx.doi.org/10.1021/acsnano.0c03801

Read Online

ACCESS | Metrics & More | Article Recommendations | Supporting Information

ABSTRACT: **Manipulation of particles in a controllable manner is highly desirable in many applications. Inspired by biological cilia, this article experimentally and numerically demonstrates a versatile particle transportation platform consisting of arrays of magnetic artificial cilia (MAC) actuated by a rotating magnet. By performing a tilted conical motion, the MAC are capable of transporting particles on their tips, along designated directions that can be fully controlled by the externally applied magnetic field, in both liquid and air, at high resolution (particle precision), with varying speeds and for a range of particle sizes. Moreover, the underlying mechanism of the controlled particle transportation is studied in depth by combining experiments with numerical simulations. The results show that the adhesion and friction between the particle and the cilia are essential ingredients of the mechanism underlying the multidirectional transportation. This work offers an advanced solution to controllably transport particles along designated paths in any direction over a surface, which has potential applications in diverse fields including lab-on-a-chip devices, *in vitro* biomedical sciences, and self-cleaning and antifouling.**

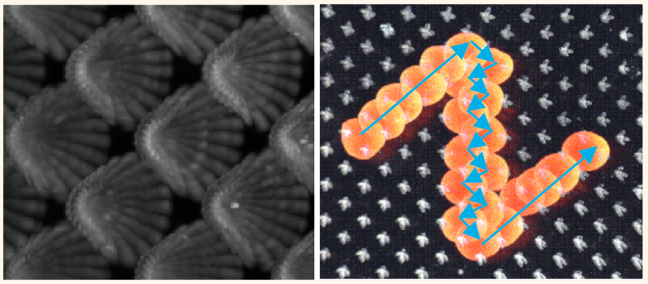

KEYWORDS: *particle manipulation, magnetic artificial cilia, directional microparticle transportation, adhesion and friction, rotating magnetic field*

Controlled manipulation of particles (both synthetic and biological) is a topic of considerable importance in fundamental and applied research such as biomedical and biochemical research,[1,2] diagnostics and therapeutics,[3] drug discovery and delivery systems,[4−6] and self-cleaning and antifouling technologies.[7−9] Specifically, in biomicrofluidics, single particle or cell manipulation enables analysis at the single cell level, revealing differences among individual cells not seen at the population level. To date, a variety of technologies has been developed to manipulate particles in fluids by acoustic, dielectrophoretic, hydrodynamic, inertial, optical, and magnetic methods or by self-propulsion.[10−18] Some methods have shown controlled 2D or even 3D particle manipulation and have made a significant impact in specific applications.[17] However, many of these methods operate within the bulk of the fluid and allow for only limited controllability of the transportation trajectory and speed. In addition, they often require that particles have specific properties or make use of an acoustic or electrical field which limits the application range. To enhance control, surface transportation can be utilized as has been achieved by robotic systems,[19,20] but these methods suffer from a rather complex design and fabrication process. Thus, it is of considerable interest, from both a scientific and a technological point of view, to create alternative methods to controllably transport individual particles over surfaces, preferably in multiple directions and in a facile way.

Inspiration to achieve this can be found in nature, where nonreciprocally beating cilia (*i.e.*, slender microscopic hair-like protrusions of cells) act to transport fluids and particles in many biological systems.[21] Specific examples are the transportation of egg cells to the uterus by motile cilia lining the inner walls of the fallopian tubes,[22] transportation of mucus and infectious agents out of the respiratory tract by motile cilia in the mammalian windpipe,[23] and directed transportation of nodal vesicle particles in the embryonic node.[24] Motivated by these examples, computational studies have been conducted to analyze the capability of artificial cilia to manipulate particles and repel fouling agents from the ciliated surface.[25−27] Recently, we experimentally demonstrated that magnetic artificial cilia (MAC) are capable of removing microparticles

Received: May 7, 2020
Accepted: July 31, 2020
Published: July 31, 2020

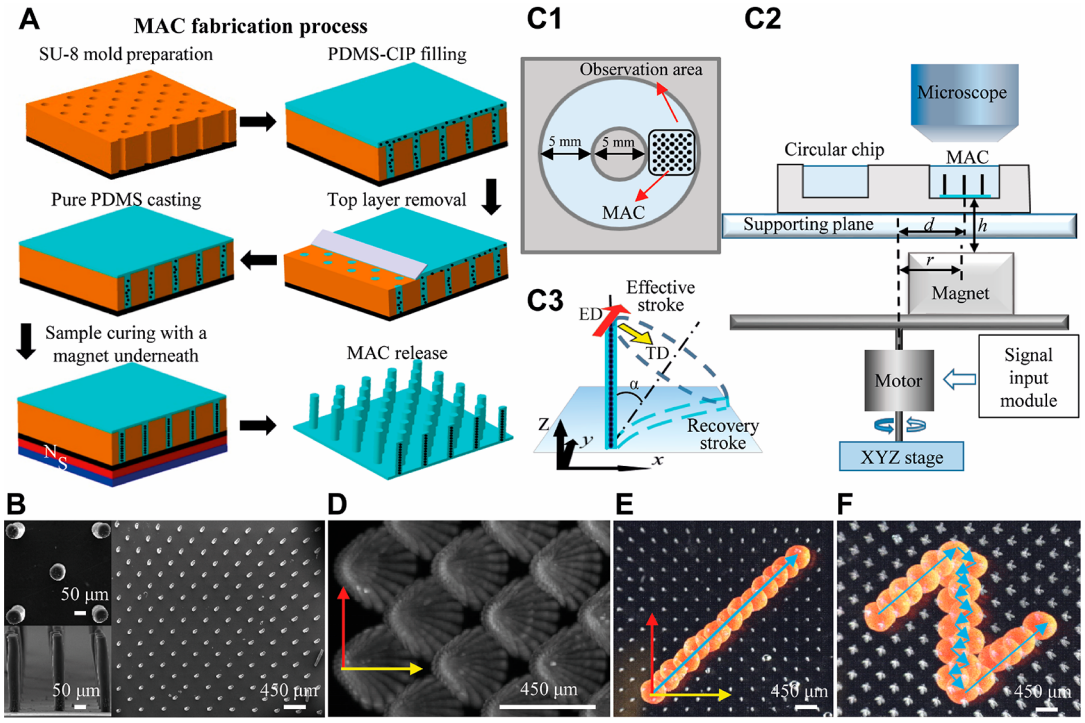

Figure 1. Experimental results, showing schematically the magnetic artificial cilia (MAC) fabrication and actuation, as well as the resulting MAC, cilia motion, and particle transportation. (A) Schematic drawing of the fabrication process of the MAC (see Materials and Methods). CIP represents the used magnetic particles carbonyl iron powder. (B) Top- and side-view scanning electron microscopy images of a fabricated MAC array; the MAC have a diameter, length, and pitch of 50, 350, and 450 μm, respectively. (C1,C2) Schematics of the actuation setup with MAC integrated in a circular-channel chip placed on a supporting plate and underneath a microscope (see Figure S1 for more details). Reproduced with permission from ref 35. Copyright 2018 Elsevier B.V. (C3) Schematic drawing of a rotating cilium performing a tilted conical motion in perspective view; the direction of the effective stroke (ED, red arrow), the tilting direction (TD, yellow arrow), and the amplitude of the cilia motion (α, in this article $\alpha = 36°$) are indicated. (D) Top view of actuated MAC: 25 superposed frames completing one full rotation cycle; the MAC perform a tilted conical motion with the effective stroke direction (red arrow) and the tilting direction (yellow arrow) as indicated in the image. (E) Top-view time-lapse trajectory of a particle transported along one direction (blue arrow) in deionized water. The particle is a 500 μm polylactic acid particle and the MAC have a pitch of 450 μm, with the cilia performing a tilted conical motion at 1 Hz; the effective stroke direction and the tilting direction are indicated in the image and are the same as in panel D. The image is an overlay of 14 images of the particle at different locations during the transportation. See Movie S1. (F) Top-view time-lapse trajectory of a transported particle along a "z"-shaped trajectory in deionized water. During this experiment, the direction of the effective stroke and the tilting direction were changed a number of times to change the direction of the particle motion. The image is an overlay of 22 images of the particle at different locations. See Movie S2.

and microalgae from the ciliated area, creating a self-cleaning and antibiofouling surface.[28,29] In addition, MAC were experimentally shown to be able to transport droplets.[30−32] Another experimental study demonstrated that MAC can be used to transport a viscoelastic particle in air, albeit at low speed (90 μm/s), not easily controlled, and only unidirectionally.[33] However, many applications require particles to be transported over a more complex trajectory in a controlled manner while still using a simple actuation system. Up to now, this has not been achieved yet.

Here, we introduce a platform based on MAC that is capable of transporting individual microparticles in a controlled manner, both in liquid and in air, multidirectionally and to any desired location. We use polylactic acid (PLA) particles with a size ranging from 400 to 800 μm as model particles. Through actuation by a rotating permanent magnet, the MAC perform a tilted conical motion, similar to that found in the embryonic node,[24] and introduced by Downton and Stark in 2009 for magnetic artificial cilia.[34] This motion leads to the continuous transportation of the particles along designated directions at a speed up to 800 μm/s. The microparticle transportation direction is determined by the combination of the rotational and tilting direction of the cilia.

To understand the underlying transport mechanism, a numerical model is used to simulate the particle manipulation over a ciliated surface. A magnetically anisotropic bead−spring model is used to model the ciliary motion. In the model, the particle interacts with the cilia by adhesive and frictional forces, while remote hydrodynamic interactions between cilia and particle are accounted for. The simulated particle behavior and trajectories agree well with the experimental results and reveal a transport mechanism based on the combination of cilia−particle interaction and cilia motion that can be fully controlled by the external magnetic field.

This work forms a major step forward compared to our earlier work.[28,29,35] In the work reported in 2018, we demonstrated the fabrication process of the MAC and showed their capability of generating versatile microfluidic flow, creating an on-chip integrated micropump.[35] In 2019, we showed how synthetic particles can be collectively removed from ciliated surfaces, due to the strong local fluid flow generated by the MAC, but in which no precise control of the direction and speed of individual particles could be achieved.[28]

https://dx.doi.org/10.1021/acsnano.0c03801
ACS Nano XXXX, XXX, XXX−XXX

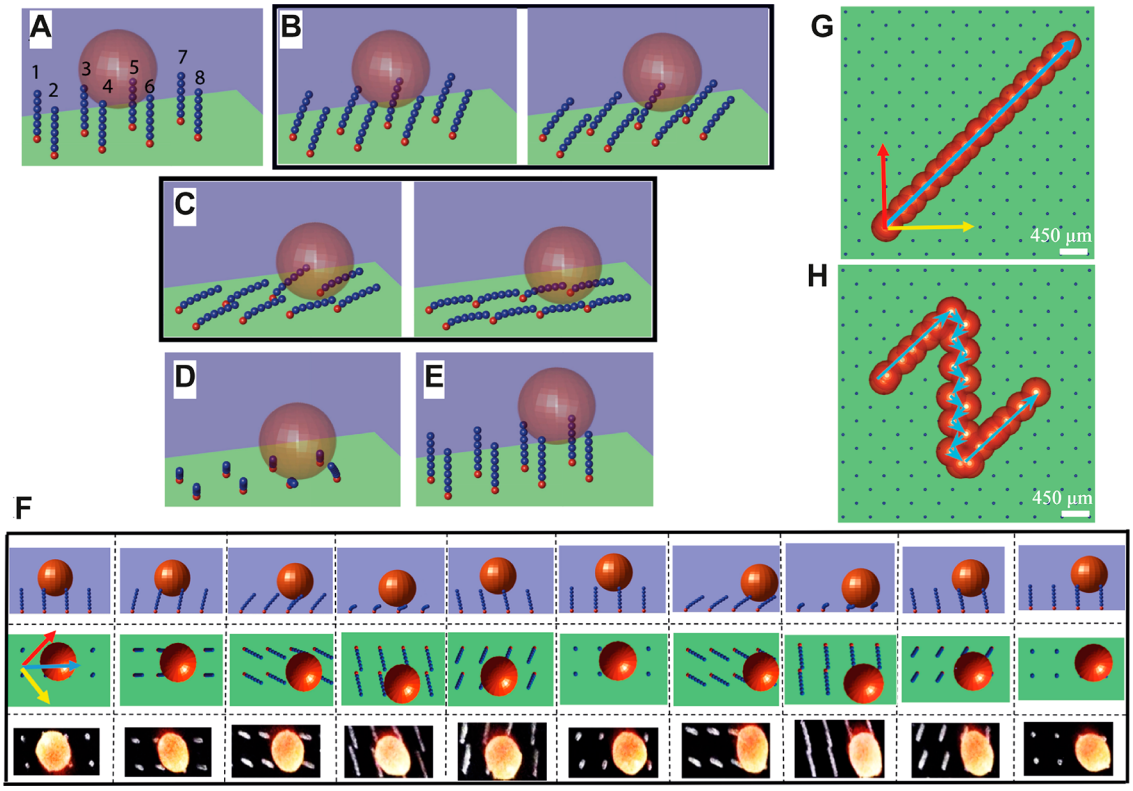

Figure 2. Particle transportation mechanism. (A–E) Perspective view of a particle transportation cycle, shown in snapshots taken from our simulations. The cilia are represented as strings of beads. The particle is made semitransparent to show the particle and cilia positions clearly—see the text for a detailed explanation. (F) Snapshots from both the simulations (top view and side view) and the experiments (top view), in which a 500 μm PLA particle is transported one cilia pitch. The red arrow, yellow arrow, and blue arrow are the effective stroke direction, cilia tilting direction, and particle transportation direction, respectively; see Movie S1. From panel A to panel F, all computational parameters are as stated in Table 1 except the adhesive strength which is $D = 8 \times 10^{-13}$ J and the cilia rotational frequency is 7 Hz. (G) Top-view time-lapse computed trajectory of a particle transported along one direction at 1 Hz; see Movie S1. (H) Top-view time-lapse computed trajectory of a transported particle along a "z"-shaped trajectory using the same protocol as in the experiment shown in Figure 1F at 7 Hz; see Movie S3. For panels G and H, all computational parameters are stated in Table 1.

Recently, we also demonstrated the capability of our MAC for creating antibiofouling and self-cleaning surfaces using a real fouling agent (microalgae).[29] The underlying mechanism in these earlier studies is the substantial flow created by the MAC motion, collectively removing the synthetic particles and microalgae from the ciliated area. In the current work, we demonstrate the fully controlled transportation of individual particles in specific directions over the ciliated surface and we study the underlying mechanism thoroughly using the combination of experiments and numerical modeling. We conclude that the key mechanism in the current method that sets it apart from our previous and other methods is the continuous contact between the MAC and the particle rather than the local flow generated by the MAC, offering enhanced control over the particle motion due to cilia–particle adhesion and friction.

RESULTS AND DISCUSSION

Experimental System and Controlled 2D Transportation of Microparticles. The artificial cilia used here are the so-called LAP MAC (magnetic artificial cilia with linearly aligned magnetic particles along the cilia's long axis) reported in our previous work.[35] The MAC, made of polydimethylsiloxane (PDMS) containing magnetic microparticles, were fabricated using a facile and reproducible micromolding process (Figure 1A). The details of the fabrication method can be found in the Materials and Methods section. The molded MAC have a cylindrical shape with a diameter of 50 μm and a height of 350 μm (Figure 1B). By fabricating molds containing microwells with different pitches, MAC arrays with a variable pitch of 350, 450, and 550 μm were created. Each cilia array consisted of $10 \times 10 + 9 \times 9 = 181$ cilia, arranged in a staggered configuration, as shown in Figure 1B.

The cilia arrays were integrated in a microfluidic chip, located on the bottom of a circular channel filled with either deionized water or air (Figure 1C1). For the particle transportation experiments, a microparticle was loaded on the ciliated surface (for details, see the Materials and Methods section). The MAC were actuated by a home-built magnetic setup (Figure 1C2 and Figure S1) to perform a tilted conical motion (Figure 1C3,D), which consists of an effective stroke when the cilium is oriented perpendicular to the surface and a recovery stroke when the cilium is moving close to the surface. As the MAC follow the externally applied magnetic field instantaneously, the revolution frequency of the MAC is identical to the rotation frequency of the motor (*i.e.*, the actuation frequency).[35] Notably, the cilia tilting direction (shown by the yellow arrow) can be modified by changing the relative location of the magnet to the cilia (*i.e.*, by changing *d* in Figure 1C2); moreover, the revolution direction of the cilia, and hence the direction of the effective stroke (shown by the

https://dx.doi.org/10.1021/acsnano.0c03801
ACS Nano XXXX, XXX, XXX–XXX

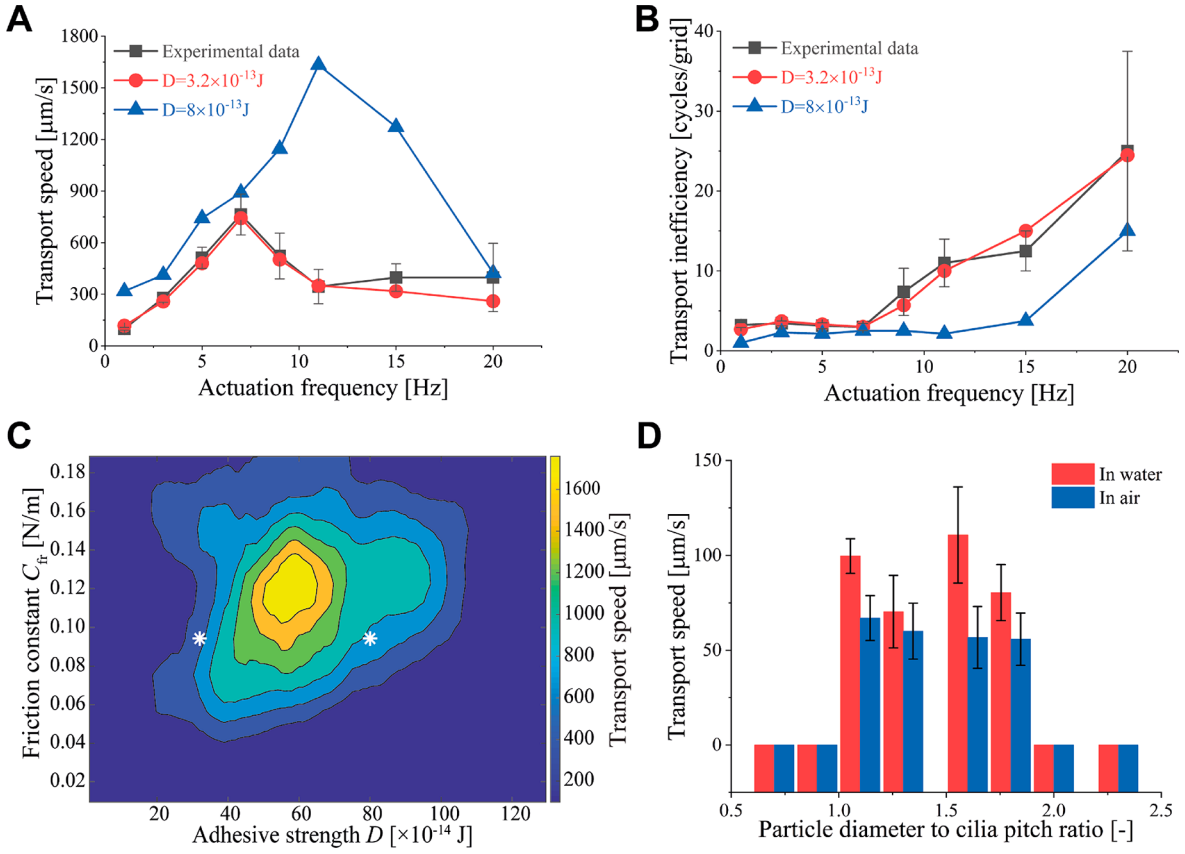

Figure 3. Transportation of PLA particles in deionized water. (A) Transportation speed as a function of the actuation frequency (equal to the rotation frequency of the cilia) for both the experiments and the numerical simulations. Each experimental data point was obtained by averaging the results of at least three identical but separately performed experiments; the error bar represents the standard deviation. The numerical results were obtained with C_{fr} = 1 × 10^{-1} N/m and two values for the adhesive strength: D = 3.2 × 10^{-13} J and D = 8 × 10^{-13} J (and all other parameters as stated in Table 1). (B) Transportation inefficiency as a function of the actuation frequency for both the experiments and the numerical simulations based on the data from panel A. This quantity is defined as the average number of rotation cycles of the cilia needed to advance the particle one cilia pitch forward. The larger the number, the less efficient the transportation. The error bars are the standard deviations of at least three identical but independent experiments. In panels A and B, the particle is a 500 μm PLA particle with a pitch of 450 μm. (C) Particle transport speed as a function of adhesive strength D and friction constant C_{fr}, as found from the numerical simulations, for a fixed actuation frequency of 7 Hz. The current experiments are best fitted using D = 3.2 × 10^{-13} J and C_{fr} = 1 × 10^{-1} N/m, indicated in the graph as the left white asterisk. The right white asterisk corresponds to D = 8 × 10^{-13} J and C_{fr} = 1 × 10^{-1} N/m. Both adhesive strengths correspond to panels A and B. All other parameters are as stated in Table 1. (D) Transportation speed as a function of the particle size to cilia pitch ratio in both water (red bars) and air (blue bars) at an actuation frequency of 1 Hz. The PLA particles have a size range from 400 to 800 μm, and the cilia arrays have a pitch of 350, 450, or 550 μm. The error bars are the standard deviations of at least three identical but independent experiments.

red arrow), can be reversed by simply reversing the rotation direction of the motor. Figure 1E shows that, through the continuous actuation of an array of cilia with a pitch of 450 μm, a 500 μm PLA particle in deionized water is transported in a direction that is determined by the directions of the effective stroke and the tilt of the cilia motion (as also shown in the Movie S1). Figure 1F shows that, by changing the effective stroke direction and the tilting direction of the MAC in a specific manner over time, the particle can be transported along different designated directions and hence can be directed to any location on top of the cilia array (see the Multidirectional Particle Transport on Ciliated Surfaces section for details; see also Movie S2).

Particle Transportation Mechanism. We developed a numerical model to validate and explain the experimental results, using the methodology described in the Materials and Methods section. In the simulations, the cilia are represented by strings of beads that are connected by springs.

The numerical results are shown in Figure 2, which displays a three-dimensional representation of the simulations, as well as snapshots of a particle being transported for one pitch length of the cilia array. At the beginning of the simulation, the particle is located in the center of a grid of four cilia, resting on top of cilia 3−6 (Figure 2A). When the cilia start performing the tilted conical motion from this time point onward, the particle moves with the cilia tips initially because of both the pushing forces from cilia 3 and 4 and the adhesive pulling forces from cilia 5 and 6 (Figure 2B, left). Subsequent bending of the cilia results in an increase in contact area between the particle and cilia 5 and 6, causing an increase of the corresponding adhesive pulling forces, whereas the contact area between the particle and cilia 3 and 4 stays approximately the same or even reduces. When the bending of the cilia is such that the forces from cilia 5 and 6 exceed the sum of adhesive and friction forces from cilia 3 and 4, the consequent net force causes the particle to separate from cilia 3 and 4 (Figure 2B, right). We have provided a brief discussion on the importance

https://dx.doi.org/10.1021/acsnano.0c03801
ACS Nano XXXX, XXX, XXX−XXX

of adhesion and friction in section SI4 of the Supporting Information (see also Movies S4 and S5). Then, the particle follows the rotation of cilia 5 and 6, making a turn (as seen from the top view in Figure 2F). During this part of the cycle, the motion of cilia 5 and 6 is hindered by the presence of the particle, which causes a distortion from the original conical trajectory for these cilia (Figure 2C, left). When the distortion reaches its maximum, the elastic energy of these cilia overcomes the constraint from the particle, and the cilia almost completely restore their alignment with the magnetic field. Meanwhile, the particle rolls around cilium 6 while adjusting its contact point with cilium 5 (Figure 2C, right). As a result, the relative position of the particle to the cilia has changed, so that the particle has made a small net forward motion. After one (or several) cycles, the particle gets into contact with cilia 7 and 8, which pull the particle further forward and constrain the particle from going back (Figure 2D). During this stage, cilia 5 and 6 can successfully slide underneath the particle so that their relative positioning with respect to the particle has now changed (compare Figure 2D with Figure 2A,B). Consequently, the particle has moved one cilia pitch forward from cilia 3−6 onto cilia 5−8 (Figure 2E). We note that the particle separation from cilia 3 and 4, the distortion of cilia 5 and 6, as well as the establishment of the adhesive contact with cilia 7 and 8 are critical to achieve effective particle transportation. Figure 2F shows a direct comparison between simulated and experimentally observed particle transportation. It may take multiple rotation cycles to transport the particle one full cilia pitch, depending particularly on the level of particle−cilia adhesion (*e.g.*, in Figure 2F it takes two cycles to transport one pitch, whereas in Figure 2A−E, it takes only one). We will get back to this important aspect in the following section on actuation frequency. A top-view time-lapse trajectory of a transported particle in water from the simulations can be found in Figure 2G,H (see also Movies S1 and 3), which agree well with the experimental results shown in Figure 1E,F.

To verify this mechanism further, we also performed experiments in which some of the cilia in the array were nonmagnetic or even removed. Details of these experiments can be found in SI5 and Movie ESI 6. These results support the mechanism described above and confirm that the directional and continuous particle transportation is realized due to the coordinated cooperation between all six neighboring cilia. The most important factors are the adhesion and friction between the particle and the cilia. If the adhesion is too strong, the particle will stay on top of four cilia permanently; on the contrary, if the adhesion is too weak, the particle will either just rotate on top of the same four cilia or be repelled from the ciliated area by the cilia-created fluid flow; see our earlier work.[28] This can be seen in Movie S7, in which the particle−cilia adhesion was reduced by adding 1 vol % sodium dodecyl sulfonate to the water. As our particle transportation system relies only on the combination of cilia motion and cilia−particle interaction and does not depend on hydrodynamic forces or inertia, the particle transportation is highly controllable. The independency of inertia is demonstrated in Movie S8, in which the effect of inertia is switched off by making the mass density of the particle equal to that of the fluid, that is, $\rho_P = \rho_{H_2O}$ (see eqs 10 and 11 in the Materials and Methods section), showing that the particle can then still be directionally transported by the MAC.

Effect of Actuation Frequency and Cilia−Particle Adhesion and Friction on Particle Transportation in Water. The transportation speed depends on the magnetic actuation frequency, equal to the revolution frequency of the MAC, as shown in Figure 3A, for a 500 μm PLA particle. The experimental results (black line) show that the transportation speed initially increases with the actuation frequency and peaks at 800 μm/s for an actuation frequency of 7 Hz, after which the speed drops at higher frequencies. Notably, the transport speed is proportional to the actuation frequency up to 7 Hz, and for these frequencies, it takes on average approximately three rotation cycles to advance the particle over one cilia grid, as shown in Figure 3B. The linear relationship between transportation speed and rotational frequency indicates that inertial effects are not at play in this frequency range. As shown in Figure 3A, the particle transportation speed is well-predicted by the numerical simulations over the complete frequency range for an adhesive strength of $D = 3.2 \times 10^{-13}$ J and a friction constant of $C_{fr} = 1 \times 10^{-1}$ N/m.

The reason for the decrease in transportation speed at higher frequencies is that it takes more and more actuation cycles for a particle to travel one cilia pitch; that is, the mechanism depicted in Figure 2 becomes less effective at higher frequencies, and more "attempts" are needed for the particle to be transported one step, as shown in Figure 3B. This is primarily due to the fact that the movement of the particle itself during each cycle decreases, for increasing frequency, by hydrodynamic drag acting on the particle, which limits particle motion and decreases cilia−particle interaction. As a result, more cycles are needed for the particle to accumulate enough displacement to get in sufficient contact with the cilia in front and move to the next cilia in the grid. By enhancing the adhesive interaction between the particle and the cilia, this effect can be counteracted. Indeed, the simulation results in Figure 3A show that, by increasing the adhesive strength D from 3.2×10^{-13} to 8×10^{-13} J, the critical frequency at which the transportation efficiency decreases is shifted to higher values, which considerably improves the transportation speed.

For a fixed frequency of 7 Hz, the quantitative effect of cilia−particle adhesion and friction on microparticle transportation speed is shown in detail in Figure 3C, obtained from numerical simulations. The particle can only be transported effectively if both the adhesion (represented by D) and the friction (represented by C_{fr}) are within a certain range, for which the force balance on the particle is suitable for moving it forward. Indeed, when in the experiments the particle−cilia adhesion was reduced by adding 1 vol % sodium dodecyl sulfonate to the water, the transportation efficiency was significantly reduced (see Movie S7), consistent with the data in Figure 3C. Figure 3C can be used as a design guideline to reach optimal transportation speeds (with an upper bound of 1700 μm/s for an actuation frequency of 7 Hz). This can be experimentally explored, for instance, by tuning the surface properties of the cilia or by adding surfactant into the liquid. The former can be done through modifying the surface hydrophobicity (i) by changing the weight ratio of the PDMS base to curing agent, (ii) by changing the curing temperature and duration, (iii) by applying a surface treatment or a coating, and (iv) by choosing other materials than PDMS. Although not investigated explicitly in this study, the stiffness of the cilia will play a role as well as this not only influences adhesion, but it also affects the motion of the cilia; in future work, the cilia bending stiffness can be tuned by tuning the geometry

https://dx.doi.org/10.1021/acsnano.0c03801
ACS Nano XXXX, XXX, XXX−XXX

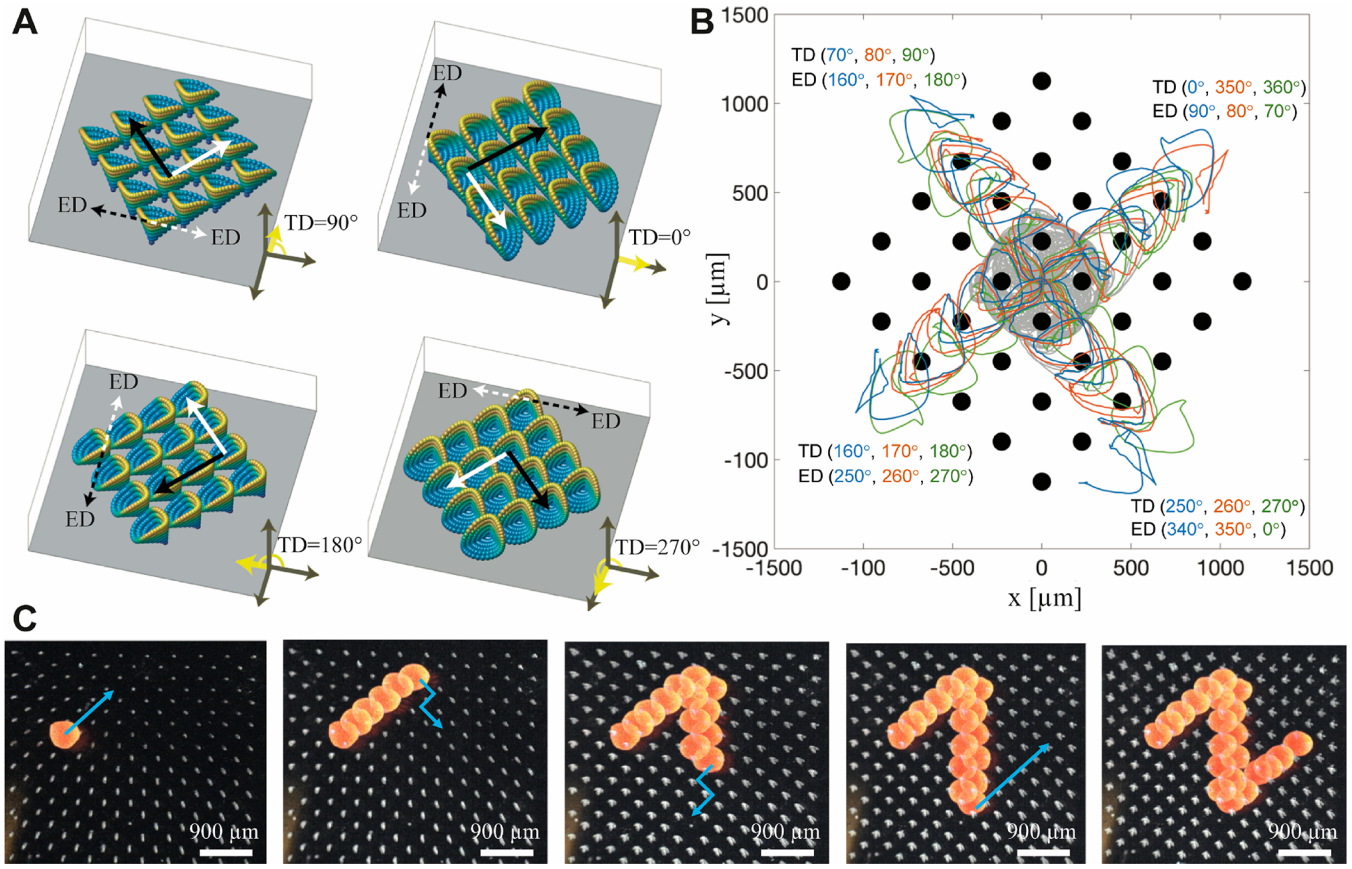

Figure 4. Multidirectional particle transportation over a ciliated surface by changing the actuation mode of the cilia. (A) Different modes of cilia motion, in which the tilting direction is varied in the four different panels between 0, 90, 180, and 270° (yellow arrow); for each TD, there are two possible effective stroke directions indicated by the dashed black and white arrows; the corresponding particle transportation directions are indicated by the solid black and white arrows. (B) Particle trajectories obtained from numerical simulations, starting at the area center, in which the tilting direction and the effective stroke direction were varied. The parameters used were those in Table 1, and the rotation frequency was 1 Hz. (C) Superposed time sequence images (top view) of a 500 μm PLA particle transported on a cilia array with a pitch of 450 μm, rotating at a frequency of 1 Hz. By changing mode of actuation between situations shown in panel A during the experiment, the particle is made to travel along a "z"-shaped trajectory (see also Movie S2, in which the effective stroke, tilting directions and particle transportation direction are shown over time). The blue arrows show particle transportation direction.

(thickness) or the elastic modulus. In addition to the properties of the cilia, the surrounding environment has an impact on the cilia–particle adhesion and friction as we will see in the next section. In addition to air and water, biofluids such as blood are also interesting media to investigate. However, as the focus of the current work is to demonstrate the controlled particle transportation and to explore the underlying generic mechanism, the testing in biofluids is out of scope of this proof-of-concept paper but forms an interesting topic for future study.

Influence of Particle Size and Cilia Pitch on Particle Transportation in Water and Air. Above, we have shown experimentally that the cilia array with 450 μm pitch is able to directionally transport a 500 μm PLA particle up to a speed of 800 μm/s in water. Here, we experimentally investigate whether the cilia array can transport particles with different sizes. To this end, we used cilia arrays with a pitch of 350, 450, or 550 μm in combination with PLA particles with a mean diameter of 400, 500, 600, 700, or 800 μm. The obtained transportation speed as a function of particle diameter to cilia pitch ratio is plotted in Figure 3D. It is clear that the cilia array has the capacity to directionally transport particles with a diameter between 1 and 2 times the cilia pitch. For these particles, the mechanism explained in Figure 2 is at work. Particles with diameters smaller than the cilia pitch (*e.g.*, with ratios smaller than 1) can only touch maximally three cilia simultaneously. As a result, they either rotate on top of the contacting cilia, they move noncontrollably, or they get stuck onto the PDMS substrate between the cilia (see Movie S9). On the other hand, particles that have a diameter of over 2 times the cilia pitch can touch more than four cilia simultaneously. Consequently, the large particles can be pulled to any direction by the surrounding cilia (see Movie S10), and therefore, the movement is less controllable.

We have also experimentally studied the transportation of the same particles in air rather than in water, which has relevant applications for particle manipulation, self-cleaning, and antifouling under dry conditions. As shown in Figure 3D, the cilia array is capable of controllably transporting PLA particles with a diameter between 1 and 2 cilia pitches in air albeit at a speed slower than that in water. That the speed is slower in air is probably because the adhesion between the particle and the cilia in air is larger than that in water, and thus more rotation cycles are needed to transport the particle one cilia grid further in air. The particles with diameters outside the 1 to 2 particle-to-pitch ratio range can still be transported but

https://dx.doi.org/10.1021/acsnano.0c03801
ACS Nano XXXX, XXX, XXX–XXX

with less control over the direction. More interestingly, particles smaller than the cilia pitch can be transported along the opposite designated direction (Movie S11). The reason is that these particles are transported directly on top of the PDMS substrate by the direct step-by-step push by the cilia approximately along the direction of the recovery stroke. The capability to transport particles in air enhances the functionality of the MAC array. The fact that, for full motion control, the particle diameter to pith ratio must be between 1 and 2 implies that the particle transportation system must be designed for specific particle sizes, which is probably very acceptable for applications in which the expected particle range is not too large.

Hence, particles of any size that have an appropriate adhesion to the cilia can be transported controllably by the cilia array with a pitch between 0.5 and 1 times the particle size. Miniaturization and scale-up of particle transportation can be realized by fabricating MAC arrays with corresponding geometrical sizes and spatial configurations. Moreover, the area of the transportation can be scaled up by fabricating larger ciliated areas and ensuring sufficient actuation of the MAC around the moving particle, for example, by readjusting the center of the rotating magnet or by creating a larger area of uniform magnetic field using an electromagnet.

Multidirectional Particle Transportation on Ciliated Surfaces. We have already demonstrated in Figure 1F and Figure 2H that we can achieve multidirectional particle transport over a ciliated surface, by changing the cilia motion during the transportation. Here, we explore this important capability of our method in more detail. Our cilia perform a rotation along a tilted cone (Figure 1C3) that is characterized by (1) the direction of the tilt of the cone along which it rotates, that is, the tilting direction, TD (yellow arrow in Figure 1C3), (2) the direction of the effective stroke, ED (red arrow in Figure 1C3), and (3) the amplitude of the cilia motion (α in Figure 1C3). In our experimental setup sketched in Figure 1C2, TD is determined by the location of the axis of rotation of the magnet with respect to the cilia (*i.e.*, d in Figure 1C2); ED is determined by the rotation direction of the magnet; α depends on the location of the magnet, the strength of the magnet, and the magnetic susceptibility of the cilia. For the direction of the particle transportation, only (1) TD and (2) ED are relevant.

For our cilia configuration, the possible combinations of TD and the ED are shown in Figure 4A. The four panels correspond to four tilting directions (yellow arrow). For each tilting direction, there are two possible effective stroke directions, indicated by the dashed black and white arrows. The corresponding particle transportation directions are indicated by the solid black and white arrows in the ciliated area. Clearly, the particle can be transported in any of the shown four directions by adjusting the tilting direction and/or the effective stroke direction, and the particle can be moved to any location in the ciliated area by shifting between the different modes.

This is demonstrated in Figure 4B that depicts results from numerical simulations. The lines shown are simulated particle trajectories, starting from the center of the area, for different directions of the tilt and effective stroke. These results also show that small deviations of 20° in TD and ED still result in controlled particle transportation along the four grid directions. Figure 4C, finally, demonstrates that, by changing TD and ED between different modes shown in panel A during the particle transportation, a particle can be directed along a predefined trajectory, in this case a "z". See also Movies S2 and S3.

In summary, the MAC array is capable of transporting individual particles along any trajectory and to any location within the ciliated area by appropriately changing the relative location of the magnet and its rotation direction during the process. More particles can be manipulated simultaneously, but as all cilia in the array are actuated synchronously, each particle will take the same trajectory (fully parallel, but shifted one or more pitch lengths relative to each other).

CONCLUSIONS

Inspired by biological cilia and by combining experiments and numerical modeling, we have demonstrated an effective strategy to transport individual particles over a surface with controllable direction and speed using an array of magnetic artificial cilia, which forms a major step forward compared to our earlier work[28,29] in which particles and microalgae were removed collectively from ciliated surfaces without the intricate motion control possible with the current method. Specifically, we have shown that, by actuating the MAC array to perform a tilted conical motion using a rotating magnet, the artificial cilia are able to transport polylactic acid particles with a diameter ranging from 1 to 2 times the cilia pitch at a speed up to 800 μm/s in water along designated directions with high controllability; the mechanism also works in air at a somewhat slower speed. The numerical simulations show that the adhesion and friction between the particles and the cilia are crucial ingredients of the mechanism of transportation, which is totally different from the working principles of our earlier work[28,29] that strongly rely on fluid flow induced by the cilia. The transportation direction is defined by the combination of tilting direction and effective stroke direction of the MAC. We have demonstrated that this system can transport particles along designated paths over the 2D ciliated area. Our proposed platform offers an alternative to existing methods in manipulating particles, with the following advantages: (1) controlled directional transport over surfaces, (2) controlled transport speed, (3) valid in both dry and wet conditions, (4) ease of control, (5) no need for applying an acoustic or electrical field, and (6) high resolution (at particle precision), but with the limitation that the cilia array must be specifically designed for particular particle sizes as well as adhesion/friction properties. Our findings provide opportunities to enhance applications in diverse fields in which control of particles (including synthetic particles, biological cells, and tissues) is relevant, including drug delivery for organ-on-a-chip applications, *in vitro* cell analyses, microfluidics, and self-cleaning and antifouling in both dry and wet conditions.

MATERIALS AND METHODS

Fabrication of Magnetic Artificial Cilia. The fabrication consisted of five steps, as shown in Figure 1A.[28,35] (1) A uniform magnetic precursor mixture consisting of PDMS (Sylgard 184, Dow Corning; base to curing agent weight ratio = 15:1) and magnetic microparticles (carbonyl iron powder, CIP, 99.5%, SIGMA-Aldrich) was poured onto a mold made of a 350 μm thick SU-8 layer with microwells patterned using photolithography, followed by a degassing procedure. The weight ratio between the PDMS and the CIP was 1:2. (2) The excess magnetic mixture outside the microwells was removed. (3) Pure PDMS (base to curing agent weight ratio = 15:1) was poured onto the mold. After being degassed, the pure PDMS layer was defined to a thickness of 150 μm by spin-coating at a rotating

https://dx.doi.org/10.1021/acsnano.0c03801
ACS Nano XXXX, XXX, XXX−XXX

speed of 400 rpm for 30 s. (4) A permanent magnet with a size of 15 × 15 × 8 mm^3 and a remnant flux density of 1.2 T was put underneath the mold in order to align the magnetic particles within the mold. The sample was left in an oven at 100 °C for 1.5 h to cure the mixture (see SI6 for details). (5) The cured pure PDMS layer with PDMS-CIP micropillars was peeled off the mold. Finally, the staggered MAC arrays with the same geometry as the mold, namely, a diameter of 50 μm and a height of 350 μm, were obtained (Figure 1B), "standing" on a transparent PDMS base substrate.

Experiments on the Particle Transportation by the MAC. Polylactic acid particles (micromod Partikeltechnologie GmbH) with diameters from 400 to 800 μm were used. The volumetric mass density of these particles is in the range of 1.1 to 1.5 g/cm^3 according to the supplier. The particle transportation experiments done in liquid were performed using the following procedure. First, using a plastic pipet, deionized water was injected slowly into the circular chip indicated in Figure 1C1 to completely fill the channel. Then, a particle was loaded on the ciliated surface using a plastic pipet. Subsequently, during experiments, the MAC were actuated by an in-house-developed magnetic actuation device (Figure 1C2 and Figure S1) to perform the tilted conical motion shown in Figure 1C3. A CMOS camera (DFK 33UX252, Imaging Source Europe GmbH) mounted on a stereomicroscope (Olympus SZ61) was used to record the movement of the particle by taking image sequences at a frame rate of 60 fps. Finally, the movement of the particle was analyzed using ImageJ. Each data point was obtained by averaging the results of at least three identically but separately performed experiments.

The experiments in air were performed in exactly the same way as those in liquid, except that the injection of deionized water was omitted.

Modeling of the Magnetic Artificial Cilia and the Cilia–Particle Interaction. In our simulations, the cilia are elastic rods with a length L_0, a circular cross-sectional area A, and Young's modulus E, which we discretize by a string of beads that are connected through linkers between the bead's centroids.[36,37] The spatial coordinates of the beads are denoted by $\boldsymbol{x}_i$, where $I = 1, ..., N$, and N (=181 × n) is the number of beads: there are 181 cilia in the analyzed cilia array with each cilium consisting of n beads. For all beads, $\boldsymbol{r}_{ij} \equiv r_{ij}\hat{\boldsymbol{r}}_{ij} = \boldsymbol{x}_j - \boldsymbol{x}_i$ denotes the connection vector pointing from bead i to j, where r_{ij} is the distance between the bead centroids and $\hat{\boldsymbol{r}}_{ij}$ is the direction unit vector. The special class of connection vectors between neighboring beads along the cilium is denoted by $\boldsymbol{t}_i \equiv \boldsymbol{r}_{(i-1)i} = l_i\hat{\boldsymbol{t}}_i$, with $\hat{\boldsymbol{t}}_i$ being the direction unit vector and l_i the distance between neighboring bead centroids.

Each ciliary bead is subjected to a magnetic force generated by the external magnetic field, a bonding force due to the neighboring cilia beads and an interaction force between the ciliary bead and the particle. As a result, the total force acting on bead i can be expressed as

$$\boldsymbol{F}_i = \boldsymbol{F}_i^{\text{magnetic}} + \boldsymbol{F}_i^{\text{bonding}} + \boldsymbol{F}_i^{\text{interaction}} \tag{1}$$

The viscous interaction with the fluid is accounted for through a hydrodynamic interaction mobility matrix (see below). The magnetic force on bead i is due to the magnetic interaction between dipole $\boldsymbol{p}_i$ and the magnetic dipoles $\boldsymbol{p}_j$ in all other ciliary beads and can be written as[38]

$$\boldsymbol{F}_i^{\text{magnetic}} = \frac{3\mu_0}{4\pi} \sum_{j\neq i} \frac{(\boldsymbol{p}_j\cdot\boldsymbol{p}_i)\hat{\boldsymbol{r}}_{ji} + \boldsymbol{p}_i(\boldsymbol{p}_j\cdot\hat{\boldsymbol{r}}_{ji}) + \boldsymbol{p}_j(\boldsymbol{p}_i\cdot\hat{\boldsymbol{r}}_{ji}) - 5\hat{\boldsymbol{r}}_{ji}(\boldsymbol{p}_i\cdot\hat{\boldsymbol{r}}_{ji})(\boldsymbol{p}_j\cdot\hat{\boldsymbol{r}}_{ji})}{r_{ji}^4} \tag{2}$$

with the dipoles in the beads being induced by the external magnetic field $\boldsymbol{B}_j$ according to[38,39]

$$\boldsymbol{p}_j = \frac{4\pi a_m^3}{3\mu_0}[\chi_{\parallel}\boldsymbol{t}_j\boldsymbol{t}_j + \chi_{\perp}(\mathbf{1} - \boldsymbol{t}_j\boldsymbol{t}_j)]\boldsymbol{B}_j \tag{3}$$

with $\mathbf{1}$ being the unity tensor and $\boldsymbol{B}_j$ the external field at the location of the bead. Here, $\chi_{\parallel}$ and $\chi_{\perp}$ are the magnetic susceptibilities along and perpendicular to the cilia axis, respectively (all cross-terms are taken to be zero); μ_0 is the permeability of free space, and a_m is the effective magnetic radius of the beads (which is not equal to the actual bead radius a_b) to account for the dipole–dipole interaction. For details on the calculation of a_m, $\chi_{\parallel}$, and $\chi_{\perp}$ the reader is referred to section SI 2 in the Supporting Information.

The bonding forces that the ciliary beads feel from the neighboring beads are due to elastic bending and stretching.[36,37] The total stretching energy of one cilium consisting of n beads can be written as

$$H^{\text{stretching}} = \frac{1}{2}k\sum_{i=2}^{n}(l_i - l_0)^2 \tag{4}$$

where l_0 is the stress-free rest length between two neighboring beads and k the stretching stiffness of an elastic rod given by EA/l_0. The first bead is assumed to be rigidly connected to the surface. Similarly, we can write the total bending energy of the cilium as

$$H^{\text{bending}} = \frac{C}{l_0}\sum_{i=2}^{n-1}(1 - \hat{\boldsymbol{t}}_{i+1}\cdot\hat{\boldsymbol{t}}_i)^2 \tag{5}$$

where C is the bending stiffness. The total bonding force acting on bead i can now be obtained from

$$\boldsymbol{F}_i^{\text{bonding}} = -\nabla_{\boldsymbol{x}_i}(H^{\text{stretching}} + H^{\text{bending}}) \tag{6}$$

where $\nabla_{\boldsymbol{x}_i}$ is the gradient operator with respect to the independent variable $\boldsymbol{x}_i$. A closed-form expression for the bonding force is given in ref 36.

The interaction force $\boldsymbol{F}_i^{\text{interaction}} = \boldsymbol{F}_i^{\text{adhesion}} + \boldsymbol{F}_i^{\text{friction}}$ accounts for the adhesive and friction forces between the cilium and the particle. The Morse potential U_{ip}^{M} is used to model the adhesive interaction between ciliary bead i and the particle (subscript p), given by[40,41]

$$U_{ip}^{M} = D[1 - e^{-\beta(r_{ip}-a_p-a_b)}]^2 \tag{7}$$

where D and β are the two Morse parameters (the adhesive strength and the adhesive interaction range, respectively), r_{ip} is the spacing between ciliary bead i and the particle, a_p is the radius of the particle, and a_b is the radius of the ciliary bead.

The adhesive interaction force between the particle and ciliary bead i is

$$\boldsymbol{F}_i^{\text{adhesion}} = -\nabla_{\boldsymbol{x}_i}((1 + g_i)U_{ip}^{M}) \tag{8}$$

where $g_i = C_{ad}(1 - \hat{\boldsymbol{r}}_{ip}\cdot\hat{\boldsymbol{t}}_i)$ is a geometrical term added to account for the difference in contact area between a continuous beam and a string of beads, with C_{ad} as a dimensionless parameter (the contact area modification constant), and $\hat{\boldsymbol{r}}_{ip}$ is the unit vector pointing from ciliary bead i to the particle. In addition, we introduce a friction force $\boldsymbol{F}^{\text{friction}}$ to describe the frictional interaction between the cilia and the particle, defined as[42−45]

$$\boldsymbol{F}_i^{\text{friction}} = C_{fr}\boldsymbol{\xi}_{ip} \tag{9}$$

where $\xi_{ip} = \xi_{ip}\hat{\boldsymbol{t}}_i$ is the shear displacement between ciliary bead i and the particle in the tangential direction defined by $\hat{\boldsymbol{t}}_i$. Here, we assume that hydrodynamic lubrication is negligible,[42] and the friction develops in a stick–slip manner that is frequently observed in the contact between particles,[43] with the friction forces and displacement irreversibly set to zero when a maximal shear displacement is attained[45] and with C_{fr} being a phenomenological friction constant.

The particle is subjected to gravity, buoyancy, and the interaction forces with the cilia, which can be written as

$$\boldsymbol{F}_p = -mg\hat{\boldsymbol{z}} - \sum_{i=1}^{N}F_i^{\text{interaction}} \tag{10}$$

https://dx.doi.org/10.1021/acsnano.0c03801
ACS Nano XXXX, XXX, XXX−XXX

with the summation accounting for all frictional and adhesion forces by the cilia, g is gravitational acceleration, and m is the buoyant mass of the particle, given by

$$m = \frac{4\pi}{3} a_p^3 (\rho_p - \rho_{H_2O}) \tag{11}$$

with a_p being the radius of the particle, ρ_p the density of the particle and ρ_{H_2O} the density of water.

For low Reynolds numbers, fluid flow is fully dominated by viscosity so that inertial effects can be neglected. In that case, the hydrodynamic coupling between the fluid, the cilia beads, and the particle is captured by the linear equations of motion:[36−38]

$$\dot{\boldsymbol{x}}_i = \sum_{j=p}^{N} \boldsymbol{\mu}_{ij} \boldsymbol{F}_j, \quad i, j = p, 1, \ldots, N \tag{12}$$

where $\boldsymbol{\mu}_{ij}$ is the mobility matrix accounting for the dynamics of the beads and particle in a viscous fluid in the neighborhood of a solid half-plane (the substrate). Here, we employ the Rotne−Prager approximation for differently sized spheres, which depends on the kinematic fluid viscosity ν.[36,38,46] Although this approximation assumes that the particles are far apart, this is not expected to significantly affect the results due to the dominance of adhesion and friction at short bead−particle distances. The differential eq 12 was solved numerically using the Euler method.[36,38]

Table 1 gives an overview of all parameters used in the computational model. The cilia and particle parameters a_b, a_p, p, and ρ_p were taken directly from the experiments. The equilibrium spring length l_0 was determined by the cilium length (L_0) and the number of beads per cilium (n). The effective magnetic bead radius a_m was calculated from the experimental CIP volume (see section SI2 in the Supporting Information for details). The magnetic strength $\boldsymbol{B}$ and susceptibility χ ($\chi_\parallel$ along the cilium, $\chi_\perp$ perpendicular to the cilium) were taken from the experimentally determined values from our earlier paper (details can be found in section SI2).[35] The stretching stiffness k was taken large enough so that the cilia do not deform axially.[36] The bending stiffness C was chosen such that the cilia perform the same motion as in the experiments, with the same maximum bending angle of 72° when exposed to the magnetic field in the experimental setup, as determined in our earlier paper (see SI3 for details).[35] The particle−cilia interaction parameters D, C_{ad}, and C_{fr} were set by fitting the computed particle transportation results to that of the experiments for a frequency of 7 Hz (see also Figure 3C). The value of β was chosen such that the length scale over which the Morse potential falls off is much smaller than the size of the particle (*i.e.*, $1/\beta \ll a_p$).[40] The best-fitted model gave $C_{ad} = 3$, an adhesive strength $D = 3.2 \times 10^{-13}$ J, and a friction constant $C_{fr} = 1 \times 10^{-1}$ N m^{-1}. The rotational frequency of the magnetic field f was varied between 1 and 20 Hz.

Table 1. Parameters Used in the Numerical Simulations

L_0	cilia length	350 μm
a_b	bead radius	25 μm
n	number of beads per cilium	7
l_0	equilibrium spring length	50 μm
a_p	particle radius	250 μm
C_{ad}	contact area modification constant	3
a_m	effective magnetic bead radius	16.7 μm
p	cilia pitch	450 μm
ρ_p	particle density	1100 kg/m^3
ρ_{H_2O}	water density	1000 kg/m^3
k	stretching stiffness	3 N/m
C	bending stiffness	1.5×10^{-14} Nm^2
C_{fr}	phenomenological friction constant	1×10^{-1} N/m
D	adhesive strength	3.2×10^{-13} J
β	adhesive interaction range	0.3 per μm
ν	kinematic viscosity	10^{-6} m^2/s

ASSOCIATED CONTENT

Supporting Information

The Supporting Information is available free of charge at https://pubs.acs.org/doi/10.1021/acsnano.0c03801.

Movie S1A: One recorded experiment together with one simulation in deionized water, showing that a 500 μm PLA particle is transported unidirectionally (MP4)

Movie S1B: Part of S1A (duration 10 s) played at 0.5 times the real speed, showing the particle transportation process in more detail (MP4)

Movie S2: One recorded experiment, showing that a 500 μm PLA particle, in deionized water, is transported along a z-shaped trajectory (MP4)

Movie S3: One recorded simulation, showing that a 500 μm PLA particle, in deionized water, is transported along a z-shaped trajectory, using the same protocol as in the experiment of S2 (MP4)

Movie S4: One recorded simulation in deionized water, showing that a 500 μm PLA particle cannot be transported without friction force at actuation frequency of 7 Hz (MP4)

Movie S5: One recorded simulation in deionized water, showing that a 500 μm PLA particle is transported unidirectionally on an 8-ciliated surface at an actuation frequency of 7 Hz for a friction constant $C_{fr} = 1 \times 10^{-1}$ N/m and an adhesive strength of $D = 8 \times 10^{-13}$J (MP4)

Movie S6A: One recorded real-time experiment in deionized water in which the cilia array contains rows of nonmagnetic cilia, showing that when cilia 3 and 4 as shown in Figure S6A are nonmagnetic, and thus no pushing forces are applied by the cilia, the 500 μm PLA particle cannot be transported (MP4)

Movie S6B: One recorded real-time experiment in deionized water in which the cilia array contains rows of nonmagnetic cilia, showing that when cilia 5 and 6 as shown in Figure S6B are nonmagnetic and thus no pulling forces are applied by the cilia directly in front of the particle, the 500 μm PLA particle cannot be transported (MP4)

Movie S6C: One recorded real-time experiment in deionized water in which the cilia array contains rows of nonmagnetic cilia, showing that when cilia 7 and 8 as shown in Figure S6C are nonmagnetic and thus cannot be actuated by the applied magnetic field, the 500 μm PLA particle can still be transported one cilia grid forward by the action of cilia 3−6, but no further (MP4)

Movie S6D: One recorded real-time experiment in deionized water in which some of the cilia are completely removed, showing that when cilia 7 and 8 as shown in Figure S6D are removed, the 500 μm PLA particle can be transported after long time actuation (around 15 s, which is 5 times the time needed to transport the particle one cilia grid forward by the normal cilia array), but no further as the particle−cilia contact is lost (MP4)

Movie S7: One recorded experiment in which the liquid is 1 vol % sodium dodecyl sulfonate which reduces the adhesion between the PLA particles and the cilia array (25), showing that a 500 μm PLA particle can only

https://dx.doi.org/10.1021/acsnano.0c03801
ACS Nano XXXX, XXX, XXX−XXX

rotate on top of the cilia and cannot be transported when the cilia rotate at 1 Hz (1−29 s) (MP4)

Movie S8: One recorded simulation in deionized water, in which the density of the PLA particle is taken equal to that of the fluid, *i.e.*, $\rho_p = \rho_{H_2O}$ showing that a 500 μm PLA particle with the same mass density as water is transported directionally (MP4)

Movie S9: One recorded experiment in deionized water, showing that the PLA particles with a diameter 400 μm, *i.e.*, smaller than the MAC pitch of 450 μm, either rotate on top of the contacting cilia, or move noncontrollably, or get stuck onto the PDMS base substrate (MP4)

Movie S10: One recorded experiment in deionized water, showing that a PLA particle with a diameter of 800 μm, larger than the MAC pitch of 350 μm, is pulled to any direction by the surrounding cilia, and thus cannot be transported controllably (MP4)

Movie S11: One recorded experiment in air, showing that the 400 μm PLA particles (smaller than the MAC pitch of 550 μm) can be transported along the direction of the recovery stroke on the PDMS substrate by the cilia direct push, contrary to the directional transportation of particle with a diameter of 1 to 2 times the cilia pitch (MP4)

Supporting figures and tables that demonstrate the actuation setup, the magnetic field experienced by the MAC, parametrization of the MAC for numerical simulations, forces acting on the transported particle, experimental verification of the particle transportation mechanism, relationship between cilia bending angle and curing duration, and supplementary movie captions (PDF)

AUTHOR INFORMATION

Corresponding Authors

Patrick R. Onck − *Zernike Institute for Advanced Materials, University of Groningen, 9747 AG Groningen, The Netherlands*; Email: P.R.Onck@rug.nl

Jaap M. J. den Toonder − *Department of Mechanical Engineering and Institute for Complex Molecular Systems, Eindhoven University of Technology, 5600 MB Eindhoven, The Netherlands*; Email: J.M.J.d.Toonder@tue.nl

Authors

Shuaizhong Zhang − *Department of Mechanical Engineering and Institute for Complex Molecular Systems, Eindhoven University of Technology, 5600 MB Eindhoven, The Netherlands*; orcid.org/0000-0002-4103-1474

Rongjing Zhang − *Zernike Institute for Advanced Materials, University of Groningen, 9747 AG Groningen, The Netherlands*

Ye Wang − *Department of Mechanical Engineering and Institute for Complex Molecular Systems, Eindhoven University of Technology, 5600 MB Eindhoven, The Netherlands*

Complete contact information is available at: https://pubs.acs.org/10.1021/acsnano.0c03801

Author Contributions

S.Z. and R.Z. contributed equally. S.Z., P.R.O., and J.M.J.dT. conceived and designed research; S.Z. and R.Z. performed the research; S.Z. and R.Z. analyzed data and wrote the paper. Y.W., P.R.O., and J.M.J.dT. revised the manuscript. The manuscript was written through contributions of all authors. All authors have given approval to the final version of the manuscript.

Notes

The authors declare no competing financial interest.

ACKNOWLEDGMENTS

We thank H. Stark and E. Gauger for kindly providing the source code of the bead−spring model that was used for the modelling. S.Z.Z. and R.J.Z. are financially supported by the China Scholarship Council under Grant Nos. 201506030055 and 201606020112, respectively. The research leading to these results has received funding from the European Research Council (ERC) under the European Union's Horizon 2020 research and innovation programme under Grant Agreement No. 833214.

REFERENCES

(1) Pamme, N. Continuous Flow Separations in Microfluidic Devices. *Lab Chip* **2007**, *7*, 1644−1659.

(2) Nilsson, J.; Evander, M.; Hammarström, B.; Laurell, T. Review of Cell and Particle Trapping in Microfluidic Systems. *Anal. Chim. Acta* **2009**, *649*, 141−157.

(3) Puri, I. K.; Ganguly, R. Particle Transport in Therapeutic Magnetic Fields. *Annu. Rev. Fluid Mech.* **2014**, *46*, 407−440.

(4) Kang, L.; Chung, B. G.; Langer, R.; Khademhosseini, A. Microfluidics for Drug Discovery and Development: From Target Selection to Product Lifecycle Management. *Drug Discovery Today* **2008**, *13*, 1−13.

(5) Dittrich, P. S.; Manz, A. Lab-On-A-Chip: Microfluidics in Drug Discovery. *Nat. Rev. Drug Discovery* **2006**, *5*, 210−218.

(6) Nguyen, N. T.; Shaegh, S. A. M.; Kashaninejad, N.; Phan, D. T. Design, Fabrication and Characterization of Drug Delivery Systems Based on Lab-On-A-Chip Technology. *Adv. Drug Delivery Rev.* **2013**, *65*, 1403−1419.

(7) Callow, J. A.; Callow, M. E. Trends in the Development of Environmentally Friendly Fouling-Resistant Marine Coatings. *Nat. Commun.* **2011**, *2*, 244.

(8) Kirschner, C. M.; Brennan, A. B. Bio-Inspired Antifouling Strategies. *Annu. Rev. Mater. Res.* **2012**, *42*, 211−229.

(9) Nir, S.; Reches, M. Bio-Inspired Antifouling Approaches: The Quest towards Non-Toxic and Non-Biocidal Materials. *Curr. Opin. Biotechnol.* **2016**, *39*, 48−55.

(10) Lu, X.; Liu, C.; Hu, G.; Xuan, X. Particle Manipulations in Non-Newtonian Microfluidics: A Review. *J. Colloid Interface Sci.* **2017**, *500*, 182−201.

(11) Laurell, T.; Petersson, F.; Nilsson, A. Chip Integrated Strategies for Acoustic Separation and Manipulation of Cells and Particles. *Chem. Soc. Rev.* **2007**, *36*, 492−506.

(12) Di Carlo, D.; Irimia, D.; Tompkins, R. G.; Toner, M. Continuous Inertial Focusing, Ordering, and Separation of Particles in Microchannels. *Proc. Natl. Acad. Sci. U. S. A.* **2007**, *104*, 18892−18897.

(13) Sing, C. E.; Schmid, L.; Schneider, M. F.; Franke, T.; Alexander-Katz, A. Controlled Surface-Induced Flows from the Motion of Self-Assembled Colloidal Walkers. *Proc. Natl. Acad. Sci. U. S. A.* **2010**, *107*, 535−540.

(14) Patra, D.; Sengupta, S.; Duan, W.; Zhang, H.; Pavlick, R.; Sen, A. Intelligent, Self-Powered, Drug Delivery Systems. *Nanoscale* **2013**, *5*, 1273−1283.

(15) Kim, K.; Guo, J.; Liang, Z.; Fan, D. Artificial Micro/Nanomachines for Bioapplications: Biochemical Delivery and Diagnostic Sensing. *Adv. Funct. Mater.* **2018**, *28*, 1705867.

(16) Zhang, S.; Wang, Y.; Onck, P.; den Toonder, J. A Concise Review of Microfluidic Particle Manipulation Methods. *Microfluid. Nanofluid.* **2020**, *24*, 24.

https://dx.doi.org/10.1021/acsnano.0c03801
ACS Nano XXXX, XXX, XXX−XXX

(17) Ozcelik, A.; Rufo, J.; Guo, F.; Gu, Y.; Li, P.; Lata, J.; Huang, T. J. Acoustic Tweezers for the Life Sciences. *Nat. Methods* **2018**, *15*, 1021−1028.
(18) Salafi, T.; Zhang, Y.; Zhang, Y. A Review on Deterministic Lateral Displacement for Particle Separation and Detection. *Nano-Micro Lett.* **2019**, *11*, 77.
(19) Palagi, S.; Fischer, P. Bioinspired Microrobots. *Nat. Rev. Mater.* **2018**, *3*, 113−124.
(20) Zhang, Z.; Wang, X.; Liu, J.; Dai, C.; Sun, Y. Robotic Micromanipulation: Fundamentals and Applications. *Annu. Rev. Control. Robot. Auton. Syst.* **2019**, *2*, 181−203.
(21) den Toonder, J. M. J.; Onck, P. R. *Artificial Cilia*; RSC Publishing: Cambridge, UK, 2013; pp 1−6.
(22) Fauci, L. J.; Dillon, R. Biofluidmechanics of Reproduction. *Annu. Rev. Fluid Mech.* **2006**, *38*, 371−394.
(23) Sleigh, M. A. Adaptations of Ciliary Systems for the Propulsion of Water and Mucus. *Comp. Biochem. Physiol. – Part A Physiol.* **1989**, *94*, 359−364.
(24) Hirokawa, N.; Okada, Y.; Tanaka, Y. Fluid Dynamic Mechanism Responsible for Breaking the Left-Right Symmetry of the Human Body: The Nodal Flow. *Annu. Rev. Fluid Mech.* **2009**, *41*, 53−72.
(25) Masoud, H.; Alexeev, A. Selective Control of Surface Properties Using Hydrodynamic Interactions. *Chem. Commun.* **2011**, *47*, 472−474.
(26) Balazs, A. C.; Bhattacharya, A.; Tripathi, A.; Shum, H. Designing Bioinspired Artificial Cilia to Regulate Particle-Surface Interactions. *J. Phys. Chem. Lett.* **2014**, *5*, 1691−1700.
(27) Tripathi, A.; Shum, H.; Balazs, A. C. Fluid-Driven Motion of Passive Cilia Enables the Layer to Expel Sticky Particles. *Soft Matter* **2014**, *10*, 1416−1427.
(28) Zhang, S.; Wang, Y.; Onck, P. R.; den Toonder, J. M. J. Removal of Microparticles by Ciliated Surfaces—An Experimental Study. *Adv. Funct. Mater.* **2019**, *29*, 1806434.
(29) Zhang, S.; Zuo, P.; Wang, Y.; Onck, P.; Toonder, J. M. J. d. Anti-Biofouling and Self-Cleaning Surfaces Featured with Magnetic Artificial Cilia. *ACS Appl. Mater. Interfaces* **2020**, *12*, 27726−27736.
(30) Yang, Z.; Park, J. K.; Kim, S. Magnetically Responsive Elastomer-Silicon Hybrid Surfaces for Fluid and Light Manipulation. *Small* **2018**, *14*, 1702839.
(31) Peng, Y.; He, Y.; Yang, S.; Ben, S.; Cao, M.; Li, K.; Liu, K.; Jiang, L. Magnetically Induced Fog Harvesting *via* Flexible Conical Arrays. *Adv. Funct. Mater.* **2015**, *25*, 5967−5971.
(32) Kim, J. H.; Kang, S. M.; Lee, B. J.; Ko, H.; Bae, W. G.; Suh, K. Y.; Kwak, M. K.; Jeong, H. E. Remote Manipulation of Droplets on a Flexible Magnetically Responsive Film. *Sci. Rep.* **2015**, *5*, 17843.
(33) Ben, S.; Tai, J.; Ma, H.; Peng, Y.; Zhang, Y.; Tian, D.; Liu, K.; Jiang, L. Cilia-Inspired Flexible Arrays for Intelligent Transport of Viscoelastic Microspheres. *Adv. Funct. Mater.* **2018**, *28*, 1706666.
(34) Downton, M. T.; Stark, H. Beating Kinematics of Magnetically Actuated Cilia. *Epl* **2009**, *85*, 44002.
(35) Zhang, S.; Wang, Y.; Lavrijsen, R.; Onck, P. R.; den Toonder, J. M. J. Versatile Microfluidic Flow Generated by Moulded Magnetic Artificial Cilia. *Sens. Actuators, B* **2018**, *263*, 614−624.
(36) Gauger, E.; Stark, H. Numerical Study of a Microscopic Artificial Swimmer. *Phys. Rev. E - Stat. Nonlinear, Soft Matter Phys.* **2006**, *74*, 021907.
(37) Gauger, E. M.; Downton, M. T.; Stark, H. Fluid Transport at Low Reynolds Number with Magnetically Actuated Artificial Cilia. *Eur. Phys. J. E: Soft Matter Biol. Phys.* **2009**, *28*, 231−242.
(38) Vilfan, M.; Potocnik, A.; Kavcic, B.; Osterman, N.; Poberaj, I.; Vilfan, A.; Babic, D. Self-Assembled Artificial Cilia. *Proc. Natl. Acad. Sci. U. S. A.* **2010**, *107*, 1844−1847.
(39) Dreyfus, R.; Baudry, J.; Roper, M. L.; Fermigier, M.; Stone, H. A.; Bibette, J. Microscopic Artificial Swimmers. *Nature* **2005**, *437*, 862−865.
(40) Bhattacharya, A.; Buxton, G. A.; Usta, O. B.; Balazs, A. C. Propulsion and Trapping of Microparticles by Active Cilia Arrays. *Langmuir* **2012**, *28*, 3217−3226.
(41) Yazdani, A.; Li, H.; Humphrey, J. D.; Karniadakis, G. E. A General Shear-Dependent Model for Thrombus Formation. *PLoS Comput. Biol.* **2017**, *13*, e1005291.
(42) Mari, R.; Seto, R.; Morris, J. F.; Denn, M. M. Shear Thickening, Frictionless and Frictional Rheologies in Non-Brownian Suspensions. *J. Rheol.* **2014**, *58*, 1693−1724.
(43) Luding, S. Cohesive, Frictional Powders: Contact Models for Tension. *Granular Matter* **2008**, *10*, 235−246.
(44) Wada, K.; Tanaka, H.; Suyama, T.; Kimura, H.; Yamamoto, T. Numerical Simulation of Dust Aggregate Collisions. I. Compression and Disruption of Two-Dimensional Aggregates. *Astrophys. J.* **2007**, *661*, 320−333.
(45) Dominik, C.; Tielens, A. G. G. M. The Physics of Dust Coagulation and the Structure of Dust Aggregates in Space. *Astrophys. J.* **1997**, *480*, 647−673.
(46) Jeffrey, D.; Onishi, Y. Calculation of the Resistance and Mobility Functions for Two Unequal Rigid Spheres in Low-Reynolds-Number Flow. *J. Fluid Mech.* **1984**, *139*, 261−290.

https://dx.doi.org/10.1021/acsnano.0c03801
ACS Nano XXXX, XXX, XXX−XXX